

---

# Eosin Y-Sensitized Partially Oxidized Ti<sub>3</sub>C<sub>2</sub> MXene for Photocatalytic Hydrogen Evolution

Yuliang Sun<sup>a</sup>, Yuan Sun<sup>a</sup>, Xing Meng<sup>a,c</sup>, Yu Gao<sup>a</sup>, Yohan Dall'Agnese<sup>a</sup>, Gang Chen<sup>a,b</sup>, Chunxiang Dall'Agnese<sup>a</sup>, Xiao-Feng Wang<sup>a,\*</sup>

<sup>a</sup>Key Laboratory of Physics and Technology for Advanced Batteries (Ministry of Education), College of Physics, Jilin University, Changchun 130012, PR China

<sup>b</sup>State Key Laboratory of Superhard Materials, Jilin University, Changchun 130012, PR China

<sup>c</sup>A. J. Drexel Nanomaterials Institute, and Department of Materials Science and Engineering, Drexel University, Philadelphia, Pennsylvania 19104, United States

Corresponding author

\*Xiao-Feng Wang: xf\_wang@jlu.edu.cn

## Abstract

Ti<sub>3</sub>C<sub>2</sub>, one of the most extensively studied 2D MXenes, is rarely reported for its potential application in dye-sensitized photocatalysis. Platinum is commonly used as co-catalyst in photocatalytic hydrogen evolution but it increases the cost and hence restricts the commercialization of this technology. Eosin Y (EY) is widely studied in dye-sensitized system as it is not only low-cost and easily commercially available, but also exhibits excellent visible light absorption ability. Herein, we oxidized Ti<sub>3</sub>C<sub>2</sub> MXene in water at 60 °C for different time, to form TiO<sub>2</sub>/Ti<sub>3</sub>C<sub>2</sub> on amorphous carbon (AC) composites. The oxidized MXene was used as photocatalyst in dye-sensitized system for hydrogen evolution to replace noble metal co-catalyst such as Pt. The highest hydrogen production rate of 33.4 μmol · h<sup>-1</sup> · g<sup>-1</sup> was achieved by TiO<sub>2</sub>/Ti<sub>3</sub>C<sub>2</sub>@AC-48h composite with the sensitization of 1 mM EY, which is 110 times higher than that of oxidized Ti<sub>3</sub>C<sub>2</sub> without EY. This work shows the potential of 2D MXenes use in dye-sensitized photocatalysis for hydrogen evolution.

---

## Introduction

Energy shortage is becoming a serious problem in the near future as the global economy growth requires increasing consumption of energy, while natural fossil fuels resources are decreasing. Solar energy is clean and has the potential to fulfill the energy gap between the consumption and the traditional energy sources. Photocatalytic water splitting for hydrogen evolution is a potential way to meet the energy demand because of both the infinite incoming sunlight and water resource. Nevertheless, the conversion of solar energy into hydrogen by catalytic process usually needs noble metal co-catalyst, such as Pt, Ru, Rh, Pd, which increases the cost of produced hydrogen energy, limiting large scale commercialization.<sup>1</sup>

The newly discovered 2D MXenes family with outstanding physicochemical properties has attracted great attention in various applications such as energy storage,<sup>2-3</sup> water purification<sup>4</sup>, electromagnetic interference shielding<sup>5</sup> and catalysis.<sup>6,7-8</sup> The general formula of MXenes is  $M_{n+1}X_nT_x$  ( $n = 1-3$ ), where M represents an early transition metal such as Ti, V, Nb, Ta and Mo, X means carbon and/or nitrogen, and T is the surface termination groups, e.g., -O, -F, -OH.<sup>9,10</sup> MXenes are produced by etching the MAX phase to remove the A element, i.e., Al and Si, using HF or similar chemicals.<sup>11,12</sup>  $Ti_3C_2$  is the most widely investigated MXenes due to its outstanding properties, such as strong connection with other semiconductors and strong interaction with  $H_2O$  molecules caused by the good hydrophilicity, high charge-carrier transfer ability induced by the excellent metallic conductivity, good redox reactivity originated from the terminal metal sites, and good stability in aqueous solutions. These distinguished natures of  $Ti_3C_2$  make it highly promising for use as a low-cost co-catalyst to replace Pt for hydrogen energy production. Hydrothermal synthesized  $TiO_2/Ti_3C_2$  nanocomposites facilitated the hydrogen evolution reaction (HER) with pure  $Ti_3C_2$  as co-catalyst.<sup>13</sup> Similarly, the hydrothermally synthesized  $TiO_2/MXenes$  composites with different mass ratios were reported for hydrogen evolution and  $TiO_2/Nb_2CT_x$  (5 wt%) showed the best performance for HER.<sup>14</sup>  $Ti_3C_2T_x$  could be oxidized by heating at 1150 °C in air for 30 seconds,<sup>15</sup> treating with  $H_2O_2$  at room temperature,<sup>16</sup> and in flowing  $CO_2$  at 850 °C,<sup>17</sup> where the resulting amorphous carbon with nano-crystalline  $TiO_2$  were used as Li-

---

ion batteries anodes. Oxidation of  $Ti_3C_2$  was also used to prepare nanocrystalline  $TiO_2$  for dye-sensitized solar cells.<sup>18</sup>

The introduction of dye molecules with visible absorption into HER can be a useful mean to improve the yield of HER, thanks to the enhancement of the light harvesting efficiency of the HER systems in which the photocatalysts are wide band gap semiconductors with poor light absorption.<sup>19</sup> In brief, the dye is excited to generate excited electrons under light irradiation. The excited electrons are injected into the conduction band of the semiconductor and finally react with  $H^+$  at the active site of the co-catalyst.<sup>20</sup> Semiconductor photocatalysts such as  $TiO_2$ ,  $ZnO$ ,  $g-C_3N_4$  are usually used in dye-sensitized HER. Transition metal-based dyes exhibits high efficiency but are not suitable for commercial and industrial applications because of the high cost and toxicity. Whereas organic dyes such as Eosin Y (EY), Rose Bengal (RB), Rhodamine B (RhB) and Methylene blue (MB) attract much attention to sensitize photocatalysts. EY is one of the most often investigated dyes due to its simple structure and commercial availability. EY and RB co-sensitized 2D graphene/Pt for HER was reported and the graphene sheets assisted separating the photogenerated electrons.<sup>21</sup> Sb doped  $SnO_2$  with different band gaps showed efficient HER under the sensitization of EY. The fast electron transfer from EY to Sb doped  $SnO_2$  contributed to the high efficiency.<sup>22</sup> EY sensitized  $g-C_3N_4/Pt/GO$  also showed increased charge separation efficiency.<sup>23</sup> Interestingly, EY sensitized  $TiO_2$  was used for photo-reduction of cadmium ion ( $Cd(II)$ ) which is a toxic element.<sup>24</sup>

Herein, we synthesized  $TiO_2/Ti_3C_2$  on amorphous carbon (AC,  $TiO_2/Ti_3C_2@AC$ ) composites by *in situ* hydrothermal oxidation in the presence of  $H_2O$  and  $O_2$ . The EY-sensitized composites were used for HER. EY was simply dissolved in water directly, which was different from the adsorbed method. The results show that the precious metal co-catalysts could be replaced by the earth abundant elements, decreasing the cost of HER technology. This work paves the way for the development of dye-sensitized photocatalysis water splitting for hydrogen production.

## Experimental section

### 2.1 The synthesis of $Ti_3C_2$ and $TiO_2/Ti_3C_2@AC$ composites

$Ti_3C_2$  MXene was prepared by etching  $Ti_3AlC_2$  (Forsman, 98%) as previously reported.<sup>25</sup> Briefly, 1 g  $Ti_3AlC_2$  was added in 10 mL HF (49%, Aladdin) in 5 minutes and stirred at a rate of 200 rpm for 24

---

hours at 30 °C. The mixture was washed by centrifugation in deionized water until the pH reached  $\approx$  7. Then the  $\text{Ti}_3\text{C}_2$  powder was dried in a vacuum oven at 60 °C overnight.

To prepare the  $\text{TiO}_2/\text{Ti}_3\text{C}_2@\text{AC}$  composites, 1 g  $\text{Ti}_3\text{C}_2$  powder was dispersed in 100 mL deionized water and kept stirring in air at 60 °C. Approximately 33 mL of the dispersion was collected after stirring for 24 h, 48 h, and 72 h, respectively. Each dispersion was centrifuged to collect the resulting powders, which was then dried in a vacuum oven at 60 °C overnight. The different composites were labeled  $\text{TiO}_2/\text{Ti}_3\text{C}_2@\text{AC}-24\text{h}$ ,  $\text{TiO}_2/\text{Ti}_3\text{C}_2@\text{AC}-48\text{h}$  and  $\text{TiO}_2/\text{Ti}_3\text{C}_2@\text{AC}-72\text{h}$ .

The EY-adsorbed sample was prepared as follows: 10 mg  $\text{TiO}_2/\text{Ti}_3\text{C}_2@\text{AC}-48\text{h}$  was dispersed by 10 mL deionized water with the EY concentration of 1mM, stirred at room temperature for 24 h, and then centrifuged and dried in a vacuum oven at 60 °C overnight.

Different EY concentrations (0.1, 0.5, 1, 2, and 5 mM) were used to optimize the hydrogen production activity of  $\text{TiO}_2/\text{Ti}_3\text{C}_2@\text{AC}-48\text{h}$  sample, and  $\text{TiO}_2$  P25 (Degussa) was used as a comparison under the optimal concentration of EY (1 mM).

## **2.2 Characterization**

The X-ray diffractometer (XRD, Bruker, D8 Advance) was operated at 40 kV and 40 mA with  $\text{Cu K}\alpha$  radiation ( $\lambda = 0.15406$  nm) to characterize the structure of  $\text{Ti}_3\text{C}_2$  and composites. The morphologies of the samples were observed by scanning electron microscopy (SEM, JSM-6700F) and high-resolution transmission electron microscopy (HRTEM, JEM-2200FS). Specific surface area was typically measured under the Brunauer-Emmer-Teller (BET) model based on  $\text{N}_2$  sorption (Kubo-X1000) with a pretreatment at 120 °C. Fourier Transform infrared spectra (FTIR, Vertex 70, Bruker, Germany) were recorded in a range of 400 to 4000  $\text{cm}^{-1}$ . Raman spectroscopy (LabRAM HR Evolution Raman Spectrometer) was carried out with a 523 nm diode-pumped solid state laser. Thermogravimetric Analysis (TGA, SDT Q600, TA, US) was tested in a range of 20 °C to 900 °C in air with a heating rate of 10 °C per min in a corundum pot and samples weight between 10 mg and 15 mg. Photoluminescence emission spectra (PL, Shimadzu RF-5301) were measured at the excitation wavelength of 340 nm and the powder samples were tested directly. Ultraviolet-visible absorption spectra (Specord 210 plus, Analytikjena, Germany) were measured for the absorption of 1  $\mu\text{M}$  EY water solution.

---

### 2.3 Photo-electrochemical activity measurements

A 6 mL photoreactor and a cut-off filter ( $\lambda > 400$  nm) were used to measure the photocatalytic hydrogen evolution under the irradiation of a 350 W xenon lamp (AHD 350, ShenzhenAnhongda Opto Technology Co. Ltd., China). The samples were controlled to be 3 mg in 3 mL aqueous solution with 29 mg/mL ascorbic acid (AA) and different concentration EY. A magnetic bar was used to disperse the composites during 6 h measurement. Argon was bubbled to remove the O<sub>2</sub> before the measurements. H<sub>2</sub> was measured by gas chromatography (SP-3420A, Beifen-Ruili, China) using argon as carrier gas. 3 mg TiO<sub>2</sub> with 1% Pt (H<sub>2</sub>PtCl<sub>6</sub>) in 29 mg/mL AA aqueous solution was used to test the hydrogen production as a comparison with and without 1 mM EY.

Electrochemical impedance spectroscopy (EIS) was performed using an electrochemical workstation (Bio - Logic SAS) over a range of 0.1 Hz to 100 kHz and an amplitude of 5 mV under the irradiation of the xenon lamp. A three-electrode configuration was used in 0.5 M Na<sub>2</sub>SO<sub>4</sub>, 11 mM AA and 0.1 mM EY aqueous electrolyte, with Ag/AgCl as the reference electrode and indium tin oxide coated glass (ITO) as the counter electrode. The working electrode was prepared by electrodeposition method, adapted from previous report<sup>26</sup>. Briefly, 40 mg of sample was dispersed in 100 mL acetone containing 20 mg dissolved I<sub>2</sub>, then a voltage of 10 V was set between two ITO electrodes for 10 min, and finally the depositional electrode was dried in an oven at 60 °C for 1 h. The ITO was washed in water and ethanol for 20 min, respectively.

## Results and discussion

### 3.1 Characterization of structures and morphology

Figure 1 shows the XRD patterns and Raman spectra of samples with different oxidation time. Obvious differences can be observed with the variation of H<sub>2</sub>O/O<sub>2</sub> treatment time in Figure 1a. Compared with the Ti<sub>3</sub>AlC<sub>2</sub> (Figure S1), the HF etched Ti<sub>3</sub>C<sub>2</sub> shows a peak down shift to  $2\theta = 9^\circ$  and lack of peak at  $39^\circ$ , demonstrating the successful removal of Al element from Ti<sub>3</sub>AlC<sub>2</sub>.<sup>25</sup> During the H<sub>2</sub>O/O<sub>2</sub> treatment at 60 °C, the titanium in Ti<sub>3</sub>C<sub>2</sub> is oxidized into TiO<sub>2</sub>, as evidenced by the appearance of the strong TiO<sub>2</sub> anatase peak at  $2\theta = 25^\circ$ . The peak at  $2\theta = 9^\circ$  nearly disappeared as the increasing

of the oxidation time, because the TiO<sub>2</sub> particles are generated on the surface of the layered material and the Ti<sub>3</sub>C<sub>2</sub> crystal structure is destroyed.

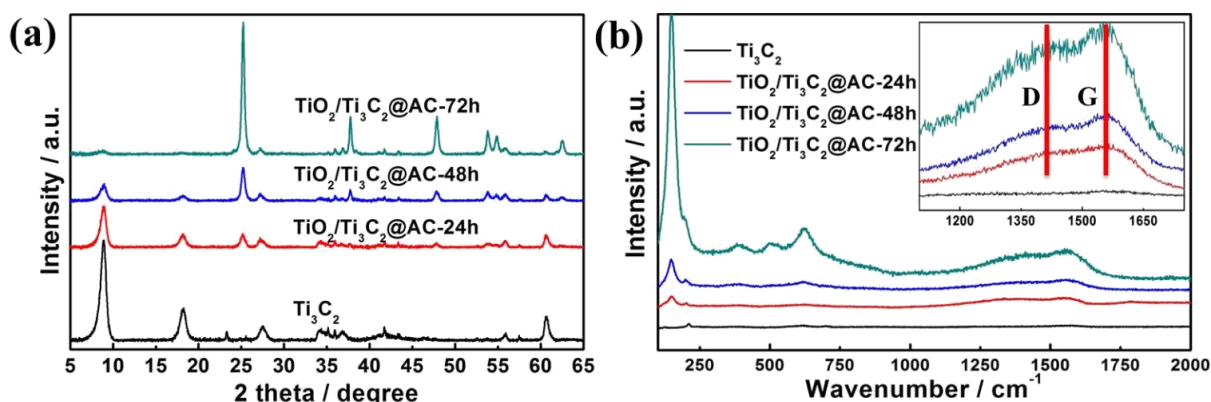


**Figure 1.** (a) The XRD and (b) Raman spectra of Ti<sub>3</sub>C<sub>2</sub>, TiO<sub>2</sub>/Ti<sub>3</sub>C<sub>2</sub>@AC-24h, TiO<sub>2</sub>/Ti<sub>3</sub>C<sub>2</sub>@AC-48h and TiO<sub>2</sub>/Ti<sub>3</sub>C<sub>2</sub>@AC-72h.

Figure 1b shows the Raman spectra of the samples. The peaks at 143 cm<sup>-1</sup> (E<sub>g</sub>), 392 cm<sup>-1</sup> (B<sub>1g</sub>), 512 cm<sup>-1</sup> (A<sub>1g</sub>+B<sub>1g</sub>) and 633 cm<sup>-1</sup> (E<sub>g</sub>) present in H<sub>2</sub>O/O<sub>2</sub> treated samples are characteristic peaks of TiO<sub>2</sub> (Figure S2), confirming the formation of anatase TiO<sub>2</sub>.<sup>15, 27, 28</sup> The mass ratio of TiO<sub>2</sub> increases as the oxidation time as evidenced by the increasing peak intensity of TiO<sub>2</sub>, which is consistent with the XRD results. The peaks at 1340 cm<sup>-1</sup> and 1550 cm<sup>-1</sup> are considered as the D- and G- bands of graphitic carbon.<sup>15, 29, 30, 31</sup> In our samples, the intensity ratios of D- and G- bands, I<sub>D</sub>/I<sub>G</sub>, are about 0.9. The ratio does not significantly change with the increase of the oxidation time, thus the amorphous carbon structure such as the disorder and defects of graphene plane are similar in all treated samples.<sup>32</sup> The formation of amorphous carbon in the oxidized samples was further demonstrated by the peaks at 561 cm<sup>-1</sup>, 586 cm<sup>-1</sup> and 651 cm<sup>-1</sup> in the FT-IR spectra (Figure S3).

Figure 2a, 2b, 2c, 2d shows the SEM images of Ti<sub>3</sub>C<sub>2</sub>, TiO<sub>2</sub>/Ti<sub>3</sub>C<sub>2</sub>@AC-24h, TiO<sub>2</sub>/Ti<sub>3</sub>C<sub>2</sub>@AC-48h and TiO<sub>2</sub>/Ti<sub>3</sub>C<sub>2</sub>@AC-72h. The layered structure of Ti<sub>3</sub>C<sub>2</sub> is clearly shown in Figure 2a. With the increasing time of H<sub>2</sub>O/O<sub>2</sub> treatment, the amount of TiO<sub>2</sub> particles increased and covered the layered Ti<sub>3</sub>C<sub>2</sub> and amorphous carbon uniformly. This morphology was obtained because the orderly arranged Ti atoms in Ti<sub>3</sub>C<sub>2</sub> were oxidized into TiO<sub>2</sub> nanoparticles.

Figure 2e, 2f shows the TEM images of the  $\text{TiO}_2/\text{Ti}_3\text{C}_2@\text{AC}$ -48h sample. The layered structure of  $\text{Ti}_3\text{C}_2$  along with the  $\text{TiO}_2$  nanoparticles can be observed.  $\text{TiO}_2$  and  $\text{Ti}_3\text{C}_2$  are identifiable in the HRTEM image by their corresponding crystal planes distances, respectively 0.37 nm and 0.26 nm<sup>33, 34</sup>.

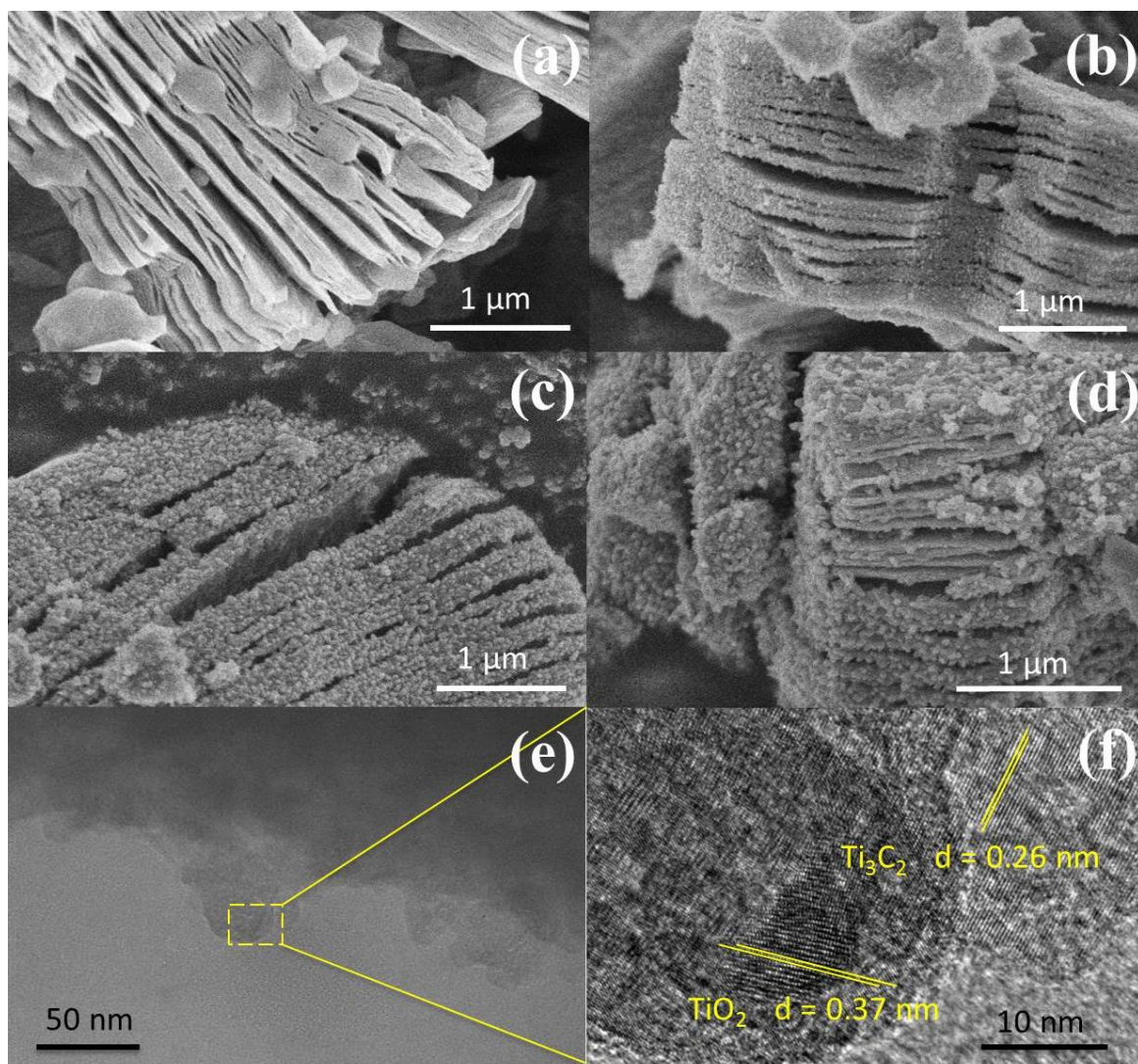


**Figure 2.** SEM images of (a)  $\text{Ti}_3\text{C}_2$ , (b)  $\text{TiO}_2/\text{Ti}_3\text{C}_2@\text{AC}$ -24h, (c)  $\text{TiO}_2/\text{Ti}_3\text{C}_2@\text{AC}$ -48h and (d)  $\text{TiO}_2/\text{Ti}_3\text{C}_2@\text{AC}$ -72h. TEM (e) and HRTEM (f) images of  $\text{TiO}_2/\text{Ti}_3\text{C}_2@\text{AC}$ -48h.

TGA of the samples were tested in air from 20 °C to 900 °C and the data are displayed in Figure 3. The mass ratio among  $\text{Ti}_3\text{C}_2$ ,  $\text{TiO}_2$ , and AC of the samples are listed in Table 1. The slight decrease before 200 °C in Figure 3a is mainly caused by removing the absorbed water and crystalline water and the change of surface termination groups in the samples.<sup>35</sup> The weight increasing above 200 °C is considered the oxidation of Ti atoms and  $\text{TiO}_2$  formation.  $\text{TiO}_2/\text{Ti}_3\text{C}_2@\text{AC}$ -72h sample shows no

increase of weight demonstrating the oxidation from  $\text{Ti}_3\text{C}_2$  to  $\text{TiO}_2$ , which is in accordance with XRD and Raman spectra. Table 1 shows consistent results that the oxidation degree of  $\text{Ti}_3\text{C}_2$  is increased with the increase of  $\text{H}_2\text{O}/\text{O}_2$  treatment time and  $\text{TiO}_2/\text{Ti}_3\text{C}_2@\text{AC}-72\text{h}$  sample is almost completely oxidized, which is in agreement with XRD and Raman results. Interestingly,  $\text{Ti}_3\text{C}_2$  shows the highest temperature of oxidation, 473 °C as shown in Figure 3b, demonstrating the better stability of  $\text{Ti}_3\text{C}_2$  than partially oxidized  $\text{Ti}_3\text{C}_2$ . As the  $\text{H}_2\text{O}/\text{O}_2$  treatment at 60 °C takes place, the titanium atoms will be soon oxidized into  $\text{TiO}_2$  at the most active flake edge of  $\text{Ti}_3\text{C}_2$ .<sup>36</sup>  $\text{TiO}_2/\text{Ti}_3\text{C}_2@\text{AC}-48\text{h}$  shows a higher oxidation temperature (370 °C) than that of  $\text{TiO}_2/\text{Ti}_3\text{C}_2@\text{AC}-24\text{h}$  (298 °C). This is mainly because there is a longer distance for  $\text{H}_2\text{O}$  and  $\text{O}_2$  to diffuse into the less active flake center of the  $\text{TiO}_2/\text{Ti}_3\text{C}_2@\text{AC}-48\text{h}$  sample to oxidize the Ti atoms of  $\text{Ti}_3\text{C}_2$ , due to the more oxidized flake edge. The amorphous carbon of  $\text{TiO}_2/\text{Ti}_3\text{C}_2@\text{AC}-72\text{h}$  was oxidized in the range of 250 °C to 900 °C, thus nearly no  $\text{Ti}_3\text{C}_2$  phase can be observed. In addition, specific surface areas (SSA) of these samples were measured and presented in Table 2. The SSA values of pure  $\text{Ti}_3\text{C}_2$  and partially oxidized samples increase with the oxidation time, because of the formation of  $\text{TiO}_2$  particles on amorphous carbon. It is interesting to see that the SSA value of  $\text{TiO}_2/\text{Ti}_3\text{C}_2@\text{AC}-72\text{h}$  is decreased in comparison to less oxidized samples, although it is the most oxidized. One possible reason is the produced  $\text{TiO}_2$  filled the space between  $\text{Ti}_3\text{C}_2$  layers. Large SSA values enhance the amount of adsorbed dye molecules and increase the number of active sites for  $\text{H}_2$  production, thus enhance the hydrogen production activity.

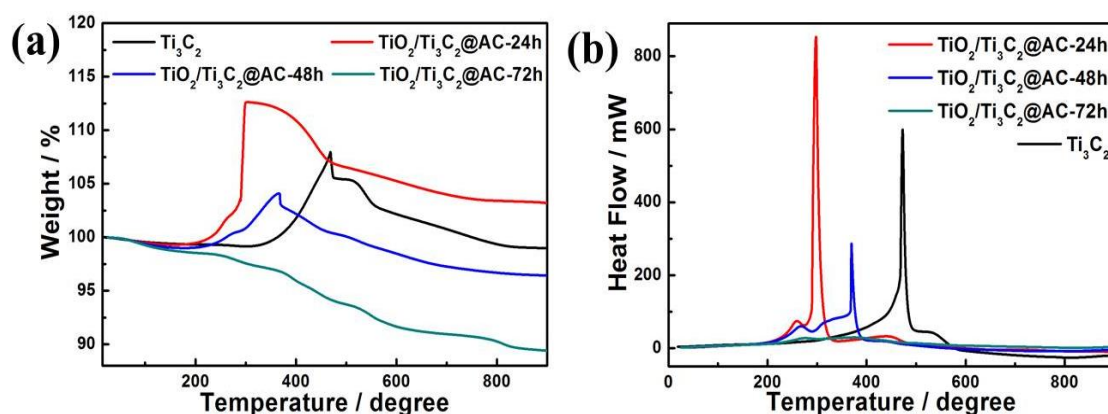


**Figure 3.** (a) The weight and (b) heat flow of TGA for  $\text{Ti}_3\text{C}_2$ ,  $\text{TiO}_2/\text{Ti}_3\text{C}_2@\text{AC}-24\text{h}$ ,  $\text{TiO}_2/\text{Ti}_3\text{C}_2@\text{AC}-48\text{h}$  and  $\text{TiO}_2/\text{Ti}_3\text{C}_2@\text{AC}-72\text{h}$ .



**Table 1.** The mass ratio (%) among Ti<sub>3</sub>C<sub>2</sub>, TiO<sub>2</sub>, and C of different samples.

Samples	Ti <sub>3</sub> C <sub>2</sub>	TiO <sub>2</sub>	C
Ti <sub>3</sub> C <sub>2</sub>	100	0	0
TiO <sub>2</sub> /Ti <sub>3</sub> C <sub>2</sub> @AC-24h	46.34	48.15	4.80
TiO <sub>2</sub> /Ti <sub>3</sub> C <sub>2</sub> @AC-48h	22.9	69.1	6.91
TiO <sub>2</sub> /Ti <sub>3</sub> C <sub>2</sub> @AC-72h	1.35	89.04	9.61

**Table 2.** Specific surface areas of different samples.

Samples	SSA (m <sup>2</sup> /g)
Ti <sub>3</sub> C <sub>2</sub>	21
TiO <sub>2</sub> /Ti <sub>3</sub> C <sub>2</sub> @AC-24h	38
TiO <sub>2</sub> /Ti <sub>3</sub> C <sub>2</sub> @AC-48h	43
TiO <sub>2</sub> /Ti <sub>3</sub> C <sub>2</sub> @AC-72h	31

### 3.2 Photo-electrochemical performance

Figure 4a shows the hydrogen production with and without EY (1 mM). Without the sensitization of EY, H<sub>2</sub> is produced as low as 0.3  $\mu\text{mol} \cdot \text{h}^{-1} \cdot \text{g}^{-1}$  by partially oxidized Ti<sub>3</sub>C<sub>2</sub>. When EY is used to sensitize the samples, the highest H<sub>2</sub> production rate of 33.4  $\mu\text{mol} \cdot \text{h}^{-1} \cdot \text{g}^{-1}$  was achieved based on the sample oxidized for 48 h, which is 110 times higher than the one without EY. This is mainly attributed to the ratio between TiO<sub>2</sub> and Ti<sub>3</sub>C<sub>2</sub>. The excited EY transfers the photo-generated electron to the TiO<sub>2</sub> and then to the surface of Ti<sub>3</sub>C<sub>2</sub>, which enhanced the charge separation of EY, thus increased the hydrogen production. The photocatalytic activity generally enhanced with the increase of SSA values. While in the TiO<sub>2</sub>/Ti<sub>3</sub>C<sub>2</sub>@AC-72h sample, when the amount of Ti<sub>3</sub>C<sub>2</sub> is very low, the hydrogen production activity decreased. This could be partially interpreted with the low amount of adsorbed dye molecules and less active sites owing to its low SSA value, leading to inefficient charge transfer. One can also see that the photocatalytic activity of pure Ti<sub>3</sub>C<sub>2</sub> sensitized with EY is better than that of TiO<sub>2</sub>/Ti<sub>3</sub>C<sub>2</sub>@AC-72h sample although it has a lower SSA value. Possible reasons are the good contact with water molecules due to its hydrophilic functionalities and efficient interfacial charge transfer

Ti<sub>3</sub>C<sub>2</sub> due to its excellent metallic conductivity. Commercial TiO<sub>2</sub> nanoparticles (P25) with 1% Pt was used as comparison with and without 1 mM EY, but only 0.7  $\mu\text{mol} \cdot \text{h}^{-1} \cdot \text{g}^{-1}$  H<sub>2</sub> production was observed with 1 mM EY, which was significantly lower than that of TiO<sub>2</sub>/Ti<sub>3</sub>C<sub>2</sub>@AC-48h.

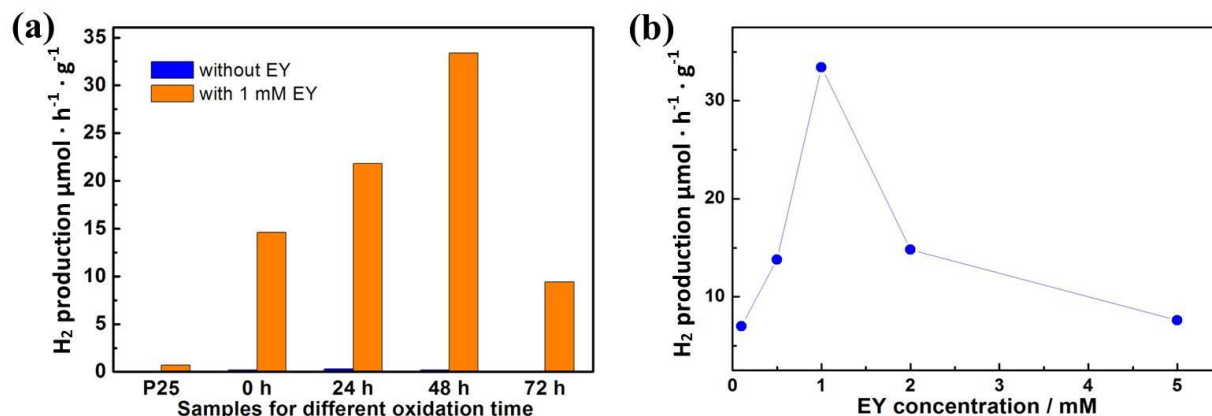


**Figure 4.** The hydrogen production for (a) Ti<sub>3</sub>C<sub>2</sub>, TiO<sub>2</sub>/Ti<sub>3</sub>C<sub>2</sub>@AC-24h, TiO<sub>2</sub>/Ti<sub>3</sub>C<sub>2</sub>@AC-48h and TiO<sub>2</sub>/Ti<sub>3</sub>C<sub>2</sub>@AC-72h with and without EY, and (b) TiO<sub>2</sub>/Ti<sub>3</sub>C<sub>2</sub>@AC-48h with different EY concentrations.

Different concentrations of EY were used to optimize the hydrogen production rate based on TiO<sub>2</sub>/Ti<sub>3</sub>C<sub>2</sub>@AC-48h sample, as shown in Figure 4b. The concentration of 1mM EY shows the best hydrogen production. The hydrogen production is increased as the concentration of EY increased from 0.1 mM to 1 mM. This is due to the enhanced adsorption of EY, leading to more photo-generated electrons transferred from EY to TiO<sub>2</sub>. When the EY concentration increases above 1 mM, the excited electrons cannot be transferred to TiO<sub>2</sub> in time. Thus, the recombination of the electron and hole generated by EY upon light absorption increases, resulting in the decrease of hydrogen production. For comparison, an EY-adsorbed sample was prepared and also used for hydrogen production. It exhibited only 1.2  $\mu\text{mol} \cdot \text{h}^{-1} \cdot \text{g}^{-1}$  H<sub>2</sub> production, much lower than samples with dissolved EY.

Figure S4 shows the EIS Nyquist plots of the samples, and the equivalent electrical circuit is shown in the inset. The fitting parameters are displayed in Table S1, which R<sub>S</sub> and R<sub>CT</sub> are the solution resistance and the interface charge-transfer resistance respectively, and CPE is the constant phase element. The result of pure Ti<sub>3</sub>C<sub>2</sub> is different from others, as it exhibits MXene pseudo-capacitive behavior (it is a well-known electrode material for supercapacitors)<sup>37</sup>, and less contribution to photo-

generated electron separation because of the lack of TiO<sub>2</sub>. The TiO<sub>2</sub>/Ti<sub>3</sub>C<sub>2</sub>@AC-48h sample has the smallest semi-circle radius among the composites, meaning the smallest interfacial charge-transfer resistance, implying a more efficient photo-generated electron transfer from EY to TiO<sub>2</sub>/Ti<sub>3</sub>C<sub>2</sub>@AC-48h, which supports the higher HER results.

Figure 5 shows the PL spectra of pure Ti<sub>3</sub>C<sub>2</sub> and the partially oxidized Ti<sub>3</sub>C<sub>2</sub> samples. The peaks near 490 nm are attributed to TiO<sub>2</sub>, as confirmed by the commercial TiO<sub>2</sub> PL spectra (Figure S5). These samples all showed the appearance of TiO<sub>2</sub>, but the TiO<sub>2</sub> peaks of TiO<sub>2</sub>/Ti<sub>3</sub>C<sub>2</sub>@AC-24h and TiO<sub>2</sub>/Ti<sub>3</sub>C<sub>2</sub>@AC-48h are weak. The strong peak of Ti<sub>3</sub>C<sub>2</sub> at 490 nm is attributed to the -O surface termination groups, forming the structure of Ti-O-Ti, which is similar to the behavior of TiO<sub>2</sub>.<sup>2</sup> The peak near 580 nm is considered the recombination of electron and hole on the amorphous carbon. A higher PL intensity means more charge recombination<sup>14, 23</sup>. The highest PL spectra intensity of TiO<sub>2</sub>/Ti<sub>3</sub>C<sub>2</sub>@AC-72h demonstrates the strongest recombination of electron and hole. This is regarded as the main reason for the lowest hydrogen production activity of TiO<sub>2</sub>/Ti<sub>3</sub>C<sub>2</sub>@AC-72h. Both Ti<sub>3</sub>C<sub>2</sub> and amorphous carbon can receive electron from TiO<sub>2</sub><sup>13, 34, 38, 39</sup> and provide active sites for hydrogen production. Compared to TiO<sub>2</sub>/Ti<sub>3</sub>C<sub>2</sub>@AC-72h with very low amount of Ti<sub>3</sub>C<sub>2</sub>, other samples show weaker PL intensities, suggesting they have more efficient charge separation. Thus TiO<sub>2</sub>/Ti<sub>3</sub>C<sub>2</sub>@AC-72h shows worse photocatalytic activity than the other three samples (Figure 4a). Besides, although TiO<sub>2</sub>/Ti<sub>3</sub>C<sub>2</sub>@AC-24h shows weaker recombination compared with TiO<sub>2</sub>/Ti<sub>3</sub>C<sub>2</sub>@AC-48h, it gives lower photocatalytic activity, which can be attributed to its lower SSA value and higher charge transfer resistance.

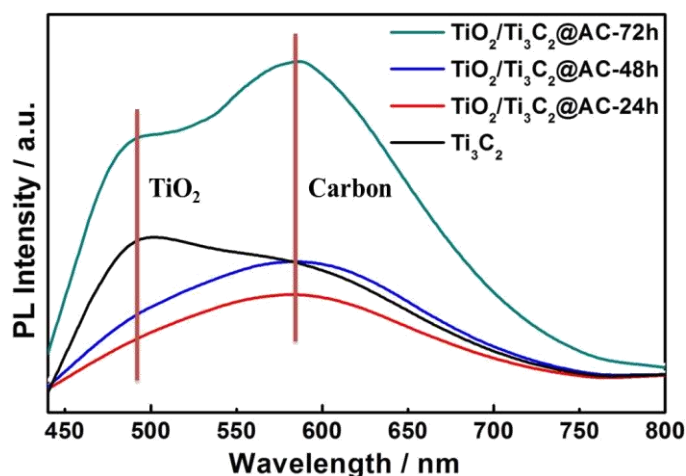


**Figure 5.** The PL spectra of  $\text{Ti}_3\text{C}_2$ ,  $\text{TiO}_2/\text{Ti}_3\text{C}_2@\text{AC}$ -24h,  $\text{TiO}_2/\text{Ti}_3\text{C}_2@\text{AC}$ -48h and  $\text{TiO}_2/\text{Ti}_3\text{C}_2@\text{AC}$ -72h.

### 3.3 Photocatalytic mechanism

To investigate the mechanism of the photocatalytic process, HOMO and LUMO levels of EY are calculated from UV-Vis absorption spectra in Figure S6. The absorption edge is observed at  $\lambda_{\text{abs}} = 540$  nm, thus the band gap of EY is 2.3 eV according to equation (1). The LUMO of EY is considered to be -3.7 eV as reported.<sup>40, 41</sup> HOMO of EY is calculated using the following equations<sup>42</sup>:

$$E_g (\text{eV}) = 1240/\lambda_{\text{abs}} (\text{nm}) \quad (1)$$

$$\text{LUMO (eV)} = \text{HOMO} + E_g \quad (2)$$

Thus, the HOMO and LUMO levels of EY are -6.0 and -3.7 eV, respectively.

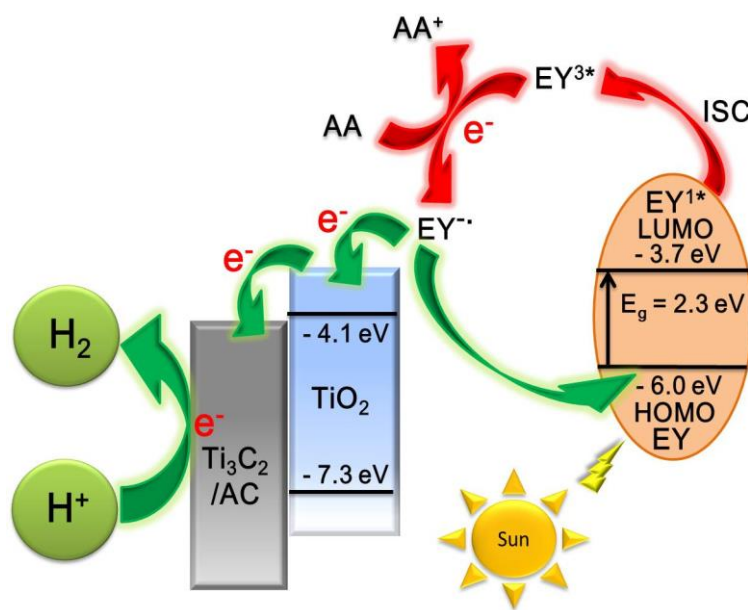


**Figure 6.** The schematic diagram of hydrogen production for EY-sensitized  $\text{TiO}_2/\text{Ti}_3\text{C}_2@\text{AC}$  composite under visible light irradiation.

A possible mechanism for EY-sensitized hydrogen production system is depicted in Figure 6. EY is excited by the visible light absorption and singlet excited state  $\text{EY}^{1*}$  is formed. Subsequently,  $\text{EY}^{1*}$  changed into lowest-lying triplet excited state  $\text{EY}^{3*}$  by an intersystem crossing (ISC) quickly. In the presence of an electron provided by AA,  $\text{EY}^{3*}$  then changed into  $\text{EY}^{\cdot-}$ .  $\text{EY}^{\cdot-}$  injects an electron into the

---

conduction band of TiO<sub>2</sub>, as the reduction potential of EY is higher than that of TiO<sub>2</sub> (- 4.1 eV).<sup>22, 35, 43</sup> The electron is finally transferred to Ti<sub>3</sub>C<sub>2</sub> and amorphous carbon to react with H<sup>+</sup> to produce H<sub>2</sub>.

## Conclusion

In conclusion, Ti<sub>3</sub>C<sub>2</sub> was partially oxidized in water at 60 °C for 24 h, 48 h and 72 h, and used in EY sensitized systems for hydrogen evolution under visible light irradiation. The hydrogen production rate of EY-sensitized composites follows the order: TiO<sub>2</sub>/Ti<sub>3</sub>C<sub>2</sub>@AC-48h > TiO<sub>2</sub>/Ti<sub>3</sub>C<sub>2</sub>@AC-24h > Ti<sub>3</sub>C<sub>2</sub> > TiO<sub>2</sub>/Ti<sub>3</sub>C<sub>2</sub>@AC-72h. This is mainly because of the different TiO<sub>2</sub>/Ti<sub>3</sub>C<sub>2</sub> ratio and the SSA values. The PL spectra demonstrated that the major reason for the low photocatalytic activity of TiO<sub>2</sub>/Ti<sub>3</sub>C<sub>2</sub>@AC-72h is due to the inefficient charge separation. EY-sensitized TiO<sub>2</sub>/Ti<sub>3</sub>C<sub>2</sub>@AC-48h shows the best hydrogen production performance with the EY concentration of 1 mM, as high as 33.4 μmol · h<sup>-1</sup> · g<sup>-1</sup>, which is 110 times higher than that of TiO<sub>2</sub>/Ti<sub>3</sub>C<sub>2</sub>@AC-48h without EY. This work gives a novel idea about Ti<sub>3</sub>C<sub>2</sub> MXene use as a co-catalyst for hydrogen production.

## Acknowledgements

This work was supported by the National Natural Science Foundation of China (No. 11574111 to X-F.W.) and Natural Science Foundation of Jilin Province (No. 20160101303JC to X-F.W.).

---

## References

1. J. Ran, J. Zhang, J. Yu, M. Jaroniec and S. Z. Qiao, *Chem. Soc. Rev.*, 2014, **43**, 7787-7812.
2. M. Naguib, J. Come, B. Dyatkin, V. Presser, P. L. Taberna, P. Simon, M. W. Barsoum and Y. Gogotsi, *Electrochem. Commun.*, 2012, **16**, 61-64.
3. N. Kurra, B. Ahmed, Y. Gogotsi and H. N. Alshareef, *Advanced Energy Materials*, 2016, **6**, 1601372.
4. Y. Ying, Y. Liu, X. Wang, Y. Mao, W. Cao, P. Hu and X. Peng, *ACS Appl Mater Interfaces*, 2015, **7**, 1795-1803.
5. F. Shahzad, M. Alhabeab, C. B. Hatter, B. Anasori, H. S. Man, C. M. Koo and Y. Gogotsi, *Science*, 2016, **353**, 1137.
6. X. Lu, K. Xu, P. Chen, K. Jia, S. Liu and C. Wu, *J. Mater. Chem. A*, 2014, **2**, 18924-18928.
7. Z. W. Seh, K. D. Fredrickson, B. Anasori, J. Kibsgaard, A. L. Strickler, M. R. Lukatskaya, Y. Gogotsi, T. F. Jaramillo and A. Vojvodic, *ACS Energy Letters*, 2016, **1**, 589-594.
8. J. Ran, G. Gao, F. T. Li, T. Y. Ma, A. Du and S. Z. Qiao, *Nat Commun*, 2017, **8**, 13907.
9. M. A. Hope, A. C. Forse, K. J. Griffith, M. R. Lukatskaya, M. Ghidui, Y. Gogotsi and C. P. Grey, *Phys. Chem. Chem. Phys.*, 2016, **18**, 5099-5102.
10. Y. Sun, D. Jin, Y. Sun, X. Meng, Y. Gao, Y. Dall'Agnese, G. Chen and X.-F. Wang, *J. Mater. Chem. A*, 2018, **6**, 9124-9131.
11. M. Naguib, V. N. Mochalin, M. W. Barsoum and Y. Gogotsi, *Adv. Mater.*, 2014, **26**, 992-1005.
12. B. Anasori, M. R. Lukatskaya and Y. Gogotsi, *Nature Reviews Materials*, 2017, **2**, 16098.
13. Y. Gao, L. Wang, A. Zhou, Z. Li, J. Chen, H. Bala, Q. Hu and X. Cao, *Mater. Lett.*, 2015, **150**, 62-64.
14. H. Wang, R. Peng, Z. D. Hood, M. Naguib, S. P. Adhikari and Z. Wu, *ChemSusChem*, 2016, **9**, 1490-1497.
15. M. Naguib, O. Mashtalir, M. R. Lukatskaya, B. Dyatkin, C. Zhang, V. Presser, Y. Gogotsi and M. W. Barsoum, *Chem Commun (Camb)*, 2014, **50**, 7420-7423.
16. B. Ahmed, D. H. Anjum, M. N. Hedhili, Y. Gogotsi and H. N. Alshareef, *Nanoscale*, 2016, **8**, 7580-7587.
17. C. J. Zhang, S. J. Kim, M. Ghidui, M.-Q. Zhao, M. W. Barsoum, V. Nicolosi and Y. Gogotsi, *Adv. Funct. Mater.*, 2016, **26**, 4143-4151.
18. C. Dall'Agnese, Y. Dall'Agnese, B. Anasori, W. Sugimoto and S. Mori, *New J. Chem.*, 2018, **42**, 16446-16450.
19. P. Chowdhury, G. Malekshoar and A. Ray, *Inorganics*, 2017, **5**, 34.
20. J. Moser and M. Graetzel, *J. Am. Chem. Soc.*, 1984, **106**, 6557-6564.
21. S. Min and G. Lu, *Int. J. Hydrogen Energy*, 2012, **37**, 10564-10574.

- 
22. L. Yang, J. Huang, L. Shi, L. Cao, W. Zhou, K. Chang, X. Meng, G. Liu, Y. Jie and J. Ye, *Nano Energy*, 2017, **36**, 331-340.
  23. P. Wang, Z. Guan, Q. Li and J. Yang, *J. Mater. Sci.*, 2017, **53**, 774-786.
  24. P. Chowdhury, S. Athapaththu, A. Elkamel and A. K. Ray, *Sep. Purif. Technol.*, 2017, **174**, 109-115.
  25. M. Naguib, M. Kurtoglu, V. Presser, J. Lu, J. Niu, M. Heon, L. Hultman, Y. Gogotsi and M. W. Barsoum, *Adv. Mater.*, 2011, **23**, 4248-4253.
  26. S. Xu, G. Wei, J. Li, Y. Ji, N. Klyui, V. Izotov and W. Han, *Chemical Engineering Journal*, 2017, **317**, 1026-1036.
  27. H. Ghassemi, W. Harlow, O. Mashtalir, M. Beidaghi, M. R. Lukatskaya, Y. Gogotsi and M. L. Taheri, *J. Mater. Chem. A*, 2014, **2**, 14339.
  28. X. Shao, W. Lu, R. Zhang and F. Pan, *Sci Rep*, 2013, **3**, 3018.
  29. A. C. Ferrari and J. Robertson, *Phys. Rev. B Condensed Matter*, 2000, **61**, 14095-14107.
  30. P. González-García, E. Urones-Garrote and L. García-González, *Mater. Chem. Phys.*, 2018, **211**, 270-277.
  31. A. Hajalilou, E. Abouzari-Lotf, V. Abbasi-Chianeh, T. R. Shojaei and E. Rezaie, *J. Alloys Compd.*, 2018, **737**, 536-548.
  32. K. Wang, J. Wang, Y. Wu, S. Zhao, Z. Wang and S. Wang, *Org. Electron.*, 2018, **56**, 221-231.
  33. R. Hao, G. Wang, C. Jiang, H. Tang and Q. Xu, *Appl. Surf. Sci.*, 2017, **411**, 400-410.
  34. C. Peng, X. Yang, Y. Li, H. Yu, H. Wang and F. Peng, *ACS Appl Mater Interfaces*, 2016, **8**, 6051-6060.
  35. Z. Li, L. Wang, D. Sun, Y. Zhang, B. Liu, Q. Hu and A. Zhou, *Materials Science and Engineering: B*, 2015, **191**, 33-40.
  36. C. J. Zhang, S. Pinilla, N. McEvoy, C. P. Cullen, B. Anasori, E. Long, S.-H. Park, A. Seral-Ascaso, A. Shmeliov, D. Krishnan, C. Morant, X. Liu, G. S. Duesberg, Y. Gogotsi and V. Nicolosi, *Chem. Mater.*, 2017, **29**, 4848-4856.
  37. Y. Dall'Agnese, P. Rozier, P.-L. Taberna, Y. Gogotsi and P. Simon, *J. Power Sources*, 2016, **306**, 510-515.
  38. C. Peng, H. Wang, H. Yu and F. Peng, *Mater. Res. Bull.*, 2017, **89**, 16-25.
  39. Y. Yang, P. Gao, Y. Wang, L. Sha, X. Ren, J. Zhang, Y. Chen, T. Wu, P. Yang and X. Li, *Nano Energy*, 2017, **33**, 29-36.
  40. Y. Wang, J. Hong, W. Zhang and R. Xu, *Cat. Sci. & Tech.*, 2013, **3**, 1703.
  41. H. Zhang, S. Li, R. Lu and A. Yu, *ACS Appl Mater Interfaces*, 2015, **7**, 21868-21874.
  42. Y. Li, W. Zhao, M. Li, G. Chen, X. F. Wang, X. Fu, O. Kitao, H. Tamiaki, K. Sakai, T. Ikeuchi and S. I. Sasaki, *Chemistry - A European Journal*, 2017, **23**, 10886-10892.
  43. C. Kong, Y. Han, L. Hou and Y. Li, *J. Photochem. and Photobio. A: Chem.*, 2017, **345**, 92-97.

## Supporting information

The XRD spectra of  $\text{Ti}_3\text{AlC}_2$  and  $\text{TiO}_2$  (anatase) were showed in supporting information. The FT-IR of different samples and Raman and PL spectra of  $\text{TiO}_2$  were also demonstrated.

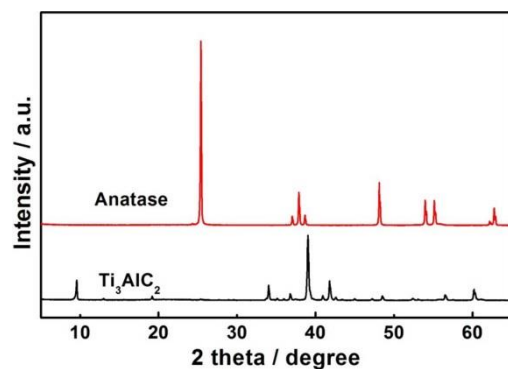


Figure S1. The XRD spectra of  $\text{Ti}_3\text{AlC}_2$  and  $\text{TiO}_2$  (anatase).

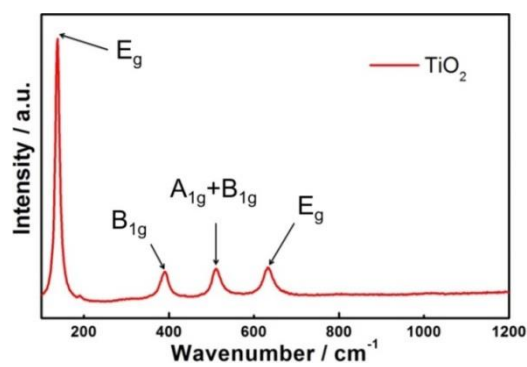


Figure S2. The Raman spectra of  $\text{TiO}_2$ .

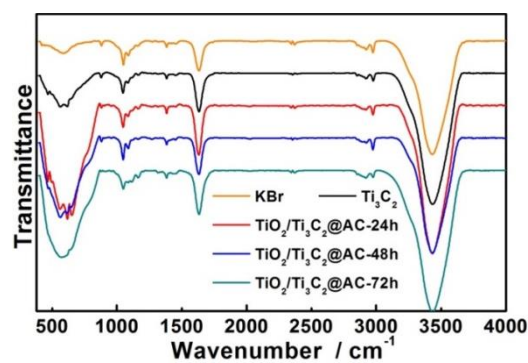


Figure S3. The FT-IR spectra of different samples.



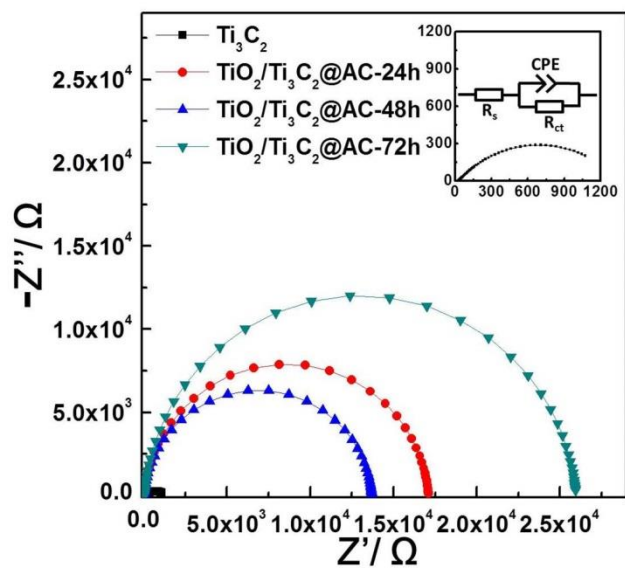


Figure S4. The Nyquist plots for  $\text{Ti}_3\text{C}_2$ ,  $\text{TiO}_2/\text{Ti}_3\text{C}_2@AC-24h$ ,  $\text{TiO}_2/\text{Ti}_3\text{C}_2@AC-48h$  and  $\text{TiO}_2/\text{Ti}_3\text{C}_2@AC-72h$ .

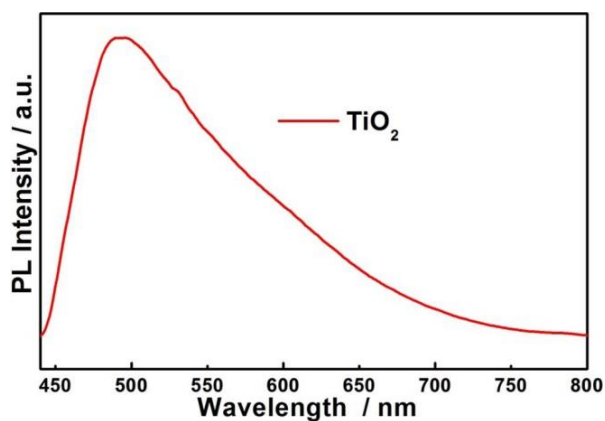


Figure S5. The PL spectra of  $\text{TiO}_2$ .

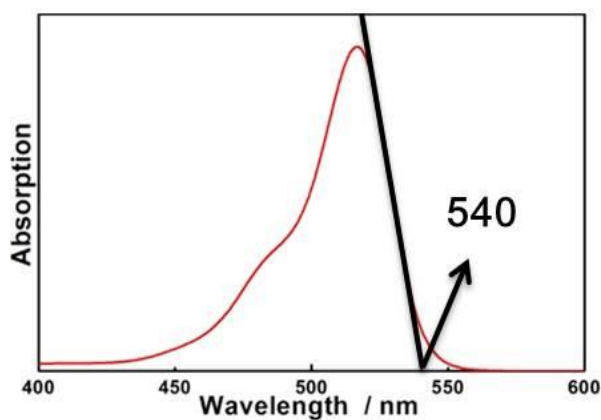


Figure S6. The absorption spectra of EY.

---

Table S1. The fitting data of Nyquist plots for  $\text{Ti}_3\text{C}_2$ ,  $\text{TiO}_2/\text{Ti}_3\text{C}_2@\text{AC-24h}$ ,  $\text{TiO}_2/\text{Ti}_3\text{C}_2@\text{AC-48h}$  and  $\text{TiO}_2/\text{Ti}_3\text{C}_2@\text{AC-72h}$ .

Samples	$R_s/\Omega$	$R_{ct}/\Omega$	CPE-P
$\text{Ti}_3\text{C}_2$	30	1319	0.52
$\text{TiO}_2/\text{Ti}_3\text{C}_2@\text{AC-24h}$	27	17086	0.95
$\text{TiO}_2/\text{Ti}_3\text{C}_2@\text{AC-48h}$	24	13678	0.95
$\text{TiO}_2/\text{Ti}_3\text{C}_2@\text{AC-72h}$	26	25932	0.95